11

DIFFUSION, BUFFERING, AND BINDING

In Chap. 9 we introduced calcium ions and alluded to their crucial role in regulating the day-to-day life of neurons. The dynamics of the free intracellular calcium is controlled by a number of physical and chemical processes, foremost among them *diffusion* and *binding* to a host of different proteins, which serve as calcium *buffers* and as calcium *sensors* or *triggers*. Whereas buffers simply bind Ca^{2+} above some critical concentration, releasing it back into the cytoplasm when $[Ca^{2+}]_i$ has been reduced below this level, certain proteins—such as calmodulin—change their conformation when they bind with Ca^{2+} ions, thereby activating or modulating enzymes, ionic channels, or other proteins.

The calcium concentration inside the cell not only determines the degree of activation of calcium-dependent potassium currents but—much more importantly—is relevant for determining the changes in structure expressed in synaptic plasticity. As discussed in Chap. 13, it is these changes that are thought to underlie learning. Given the relevance of second messenger molecules, such as Ca^{2+}, IP_3, cyclic AMP and others, for the processes underlying growth, sensory adaptation, and the establishment and maintenance of synaptic plasticity, it is crucial that we have some understanding of the role that diffusion and chemical kinetics play in governing the behavior of these substances.

Today, we have unprecedented access to the spatio-temporal dynamics of intracellular calcium in individual neurons using *fluorescent calcium dyes*, such as fura-2 or fluo-3, in combination with *confocal* or *two-photon microscopy* in the visible or in the infrared spectrum (Tsien, 1988; Tank et al., 1988; Hernández-Cruz, Sala, and Adams, 1990; Ghosh and Greenberg, 1995). The data gleaned from these methods of directly visualizing calcium in the dendritic tree, cell body, and presynaptic terminals are quantitative enough to allow detailed comparison with numerical models, commencing with the work of Hodgkin and his colleagues in the squid axon (Blaustein and Hodgkin, 1969; Baker, Hodgkin, and Ridgway, 1971) and continuing with the study of calcium transients in the presynaptic terminal (Llinás, Steinberg and Walton, 1981a,b; Zucker and Stockbridge, 1983; Stockbridge and Moore, 1984; Simon and Llinás, 1985; Zucker and Fogelson, 1986; Parnas, Hovav, and Parnas, 1989; Yamada and Zucker, 1992) as well as in dendrites, cell bodies and spines (Connor and Nikolakopoulou, 1982; Gamble and Koch, 1987; Sala and Hernández-Cruz, 1990; Holmes

and Levy, 1990; Carnevale and Rosenthal, 1992; Zador and Koch, 1994; DeSchutter and Bower, 1994a,b; DeSchutter and Smolen, 1998; Borg-Graham, 1998; Yamada, Koch, and Adams, 1998).

In this chapter, we study the physics of diffusion and buffering, dwelling at some length on the fundamental limitations imposed by physics on how fast substances can diffuse. We will develop certain analogies between the reaction-diffusion equation and the cable equation and discuss the potential relevance of these processes for information processing and computation. While these results apply to any substance diffusing inside cells and binding to other molecules, we will focus on Ca^{2+} ions, given their crucial role in the day-to-day life of neurons and, in fact, in all cells. The control and regulation of calcium in neuronal structures is a vast subject, which we can only briefly hint at. For more details on calcium signaling in neurons the reader is urged to consult Hille's monograph (1992), the articles by Ghosh and Greenberg (1995) and by Clapham (1995), or the insightful Meyer and Stryer (1991) review. Finally, for the computational methods, consult DeSchutter and Smolen (1998). We end by discussing some general aspects of information processing using calcium.

Let us commence by deriving the diffusion equation that underlies the distribution of ions inside and outside cells.

11.1 Diffusion Equation

Historically, the diffusion equation was first derived from a macroscopic, deterministic point of view by Fick (1855), who postulated a force arising between molecules proportional to their concentration difference. Although such a phenomenological approach does lead to the correct equation, we now know that no such force exists. Instead, diffusion is due to the constant agitation of molecules arising from their thermal energy. The physically correct probabilistic interpretation of this *Brownian motion* was advanced by Einstein (1905), who used the theory of random walk. Because of the simplicity and elegance of his arguments, we will develop here a heuristic derivation of the diffusion equation using this stochastic perspective.

11.1.1 Random Walk Model of Diffusion

The starting point of the molecular theory of heat is that molecules and small particles at the absolute temperature T have, on average, a kinetic energy $kT/2$ associated with movement along each dimension. The resulting velocities of these particles in solution do not allow them to travel very far since they collide within picoseconds with other molecules, changing their direction of travel as a result. This incessant and random agitation of molecules due to thermal energy is the basis of diffusion.

Imagine a particle moving along an one-dimensional line. Both space and time are discretized, such that the particle can only be at locations $\pm m\Delta x$, where m is an integer. Each time step Δt, the particle can move either with 50% probability to the right or with 50% probability to the left, in both cases by the amount Δx. The particle cannot remain in place or move by more than Δx. Finally, we assume that the particle has no memory of any locations it has previously visited.

These rules allow us to define a probability distribution $p(x, t)$ that the particle will be at position x at time t. The only way the particle could have arrived at position x is if it was at either one of the two adjacent positions in the previous time step. That is,

$$p(x,t) = \frac{1}{2}\left(p(x-\Delta x, t-\Delta t) + p(x+\Delta x, t-\Delta t)\right) . \tag{11.1}$$

Subtracting $p(x, t-\Delta t)$ from both sides as well as dividing by Δt yields

$$\frac{p(x,t)-p(x,t-\Delta t)}{\Delta t} =$$

$$\frac{(\Delta x)^2}{2\Delta t}\,\frac{p(x-\Delta x, t-\Delta t) - 2p(x,t-\Delta t) + p(x+\Delta x, t-\Delta t)}{(\Delta x)^2} \tag{11.2}$$

The left-hand side of this equation is nothing but the first-order approximation of the first temporal derivative of p, while the term on the right-hand side corresponds to the second-order approximation of the second spatial derivative of $p(x, t-\Delta t)$. In the limit as Δx and Δt approach zero in such a way that

$$\frac{(\Delta x)^2}{2\Delta t} = D \tag{11.3}$$

converges toward a finite constant (with units of cm^2/sec), we end up with the partial differential *diffusion equation*

$$\frac{\partial p(x,t)}{\partial t} = D\frac{\partial^2 p(x,t)}{\partial x^2} . \tag{11.4}$$

It describes how the probability function $p(x, t)$ evolves over time and is also known under the generic name of *Fokker-Planck equation*. We will reencounter this class of equations in Chap. 15.

The simplest interpretation of diffusion can be given if the single particle is replaced by a cloud of N independently moving particles that all start off at the origin, $x = 0$. What is the expected mean position of this cloud of particles and the variance around this mean position? According to our simple model, $x_i(t)$ for particle i at time $t = n\Delta t$ can only differ from the previous position by $\pm\Delta x$,

$$x_i(n\Delta t) = x_i((n-1)\Delta t) \pm \Delta x . \tag{11.5}$$

The average position of the cloud, $\langle x(n\Delta t)\rangle$, at time $n\Delta t$ is given by summing over all the individual particles,

$$\langle x(n\Delta t)\rangle = \frac{1}{N}\sum_{i=1}^{N} x_i(n\Delta t) = \frac{1}{N}\sum_{i=1}^{N}[x_i((n-1)\Delta t) \pm \Delta x] . \tag{11.6}$$

Since we assumed earlier that each particle has an equal chance of moving to the left or to the right (and that no boundaries impede the motion of the particles), the last term in brackets averages zero for large numbers of particles. This equation then tells us that the mean position of the cloud at time $n\Delta t$ does not change from its previous position, $\langle x(n\Delta t)\rangle = \langle x((n-1)\Delta t)\rangle$. If the cloud starts off at the origin, we conclude that the average location of the cloud will never move,

$$\langle x(n\Delta t)\rangle = 0 . \tag{11.7}$$

If we incorporate a systematic drift into the motion of the particles, for instance, by applying an electric field that imposes a preferred direction of motion (assuming that the moving

particle is charged), this result will have to be modified. However, in the absence of such a bias, the cloud will remain centered at the origin.

How much does the cloud spread out over time? As anybody can observe when placing a drop of ink into a water glass, at first a small part of the water is stained an intense blue. Later on, the spot of blue becomes less intense and larger, dispersing eventually throughout the entire glass. One measure of this spreading is the variance of the mean position of the cloud. This is defined as

$$\begin{aligned}\langle x(n\Delta t)^2\rangle &= \frac{1}{N}\sum_{i=1}^{N} x_i(n\Delta t)^2 \\ &= \frac{1}{N}\sum_{i=1}^{N}[x_i((n-1)\Delta t)^2 \pm 2\Delta x \cdot x_i((n-1)\Delta x) + (\Delta x)^2]\end{aligned} \tag{11.8}$$

(we here used Eq. 11.5). Because the random walk is unbiased, the second term in this equation will be zero on average, resulting in

$$\langle x(n\Delta t)^2\rangle = \langle x((n-1)\Delta t)^2\rangle + (\Delta x)^2 . \tag{11.9}$$

We can, of course, recursively apply the same decomposition for $\langle x((n-1)\Delta t)^2\rangle$, ending up in n steps with $\langle x(0)^2\rangle$. Since the entire population started out at the origin, this last term in zero. Setting $t = n\Delta t$ and remembering that $(\Delta x)^2/(2\Delta t) = D$, we conclude

$$\langle x(t)^2\rangle = 2Dt . \tag{11.10}$$

Thus, while the mean position of the cloud does not move, the variance or width of the cloud increases linearly with time and its standard deviation as the square root of time. Interpreted in terms of single particles, Eq. 11.7 implies that the mean position of a single particle does not change while the probability of finding it at larger and larger distances from the origin increases as the square root of time (Eq. 11.10).

11.1.2 Diffusion in Two or Three Dimensions

The same concept can be applied to the motion of a particle in more than one dimension. As long as the motion along the x direction is independent of the motion in the y direction, the variance of motion in the plane is the sum of the variances of motion in the two independent directions,

$$\langle r(t)^2\rangle = \langle x(t)^2\rangle + \langle y(t)^2\rangle = 4Dt . \tag{11.11}$$

A computer simulation of such a random walk is illustrated in Fig. 11.1. Given the square-root relationship between time and distance traversed, it is possible for the particle to explore short distances much more thoroughly than large distances. Thus, the typical pattern evident in Fig. 11.1: the particle tends to return to the same region many times before eventually wandering away. When it does move away, it blindly chooses another region to explore, with no regard for whether or not it had previously visited that area. This reflects the fact that the particle does not move down any gradient in response to a "diffusive" force as postulated by Fick (1855), but acts in a probabilistic manner to spread over the available space; its tracks do not uniformly fill up the available space. For a particle diffusing in three dimensions, exactly the same principle applies, except that now

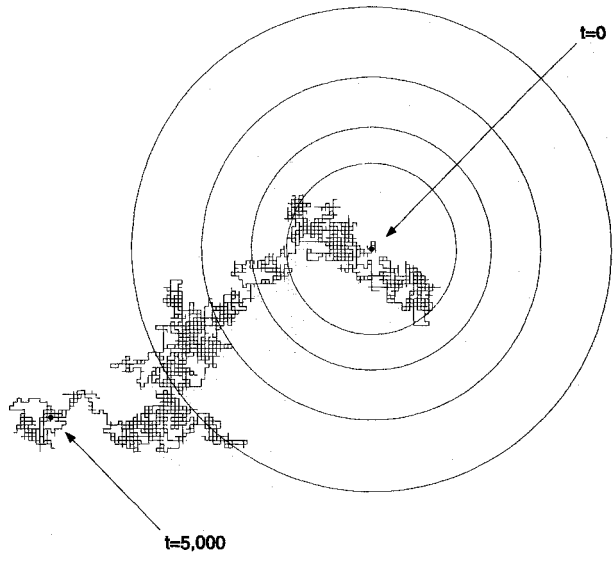

Fig. 11.1 DIFFUSION OF A PARTICLE IN THE PLANE Computer simulation of a single particle executing a random walk on a rectangular grid. At each point in time, it has a probability of 0.25 of moving in any one of four directions. In the limit of an infinitesimally fine grid, this approximates diffusion in a plane. The particle started at the center and after 5000 iterations ended up at the lower left corner. The radii of the four circles correspond to the variance in the locations of the particle after 500, 1000, 2000, and 4000 iterations. The expected time-averaged location of the particle is always at the center of the bull's eye.

$$\langle r(t)^2 \rangle = \langle x(t)^2 \rangle + \langle y(t)^2 \rangle + \langle z(t)^2 \rangle = 6Dt\,. \tag{11.12}$$

The *random walk* approach to diffusion has been very fruitful in mathematical physics. It is straightforward to derive equations corresponding to particles moving down a gradient caused, for instance, by an applied electric field, or if the space the particle moves in has absorbing or reflecting boundaries such as a membrane. For more details on the mathematics of random walk see the idiosyncratic, but immensely informative, monograph by Mandelbrot (1977); for a delightful text on the use of random walk techniques to describe the motion of bacteria and other small organisms see Berg (1983).

11.1.3 Diffusion Coefficient

In the above, we assumed—see Eq. 11.3—that D is purely dictated by the temporal and spatial discretization steps. However, for real particles in solution—where gravity can be neglected—D must clearly depend on certain physical attributes of the particles themselves as well as on properties of the solution. What precisely determines D and how large is it for real ions, such as Ca^{2+}, and big molecules, such as calmodulin which binds free Ca^{2+} in neurons?

Einstein (1905), arguing that diffusion is thermal agitation of particles opposed by friction, derived a general relationship between diffusion and friction. For particles that can be approximated as spheres much larger than the size of individual water molecules (which are on the order of 1 Å), D is determined by the *Einstein-Stokes relation* as

$$D = \frac{kT}{6\pi\eta r_S} \tag{11.13}$$

where r_S is the radius of the diffusing particle and η the viscosity of water. The proportionality of D to the absolute temperature T simply reflects the thermal origin of diffusion. For room temperature (20° C), this equation reduces to $D = \alpha/r_S$, with $\alpha = 2.15\ \mu m^2/msec$ and the radius r_S specified in units of angstrom (Å). (For a very thorough discussion of this, see Hille, 1992.) The diffusion coefficient is usually specified in cm^2/sec; however, we will adopt units more convenient to neuronal structures and measure D in units of $\mu m^2/msec$.

The Einstein-Stokes relationship—based on classical hydrodynamics— is accurate for large particles, but works less well for small ions. For instance, for the 0.99 Å radius calcium ion, D should be 2.14 $\mu m^2/msec$ but is, in fact, 0.6 $\mu m^2/msec$ (Blaustein and Hodgkin, 1969). This mismatch is partially caused by the formation of a hydration shell around the ion, that is, water molecules that lie in direct contact with each ion in solution. For larger and heavier molecules, this is less of a consideration and their radius can be thought of as being approximately proportional to the cubic root of their molecular weight. Table 11.1 lists the diffusion coefficients of a number of ions and molecules for diffusion in an aqueous medium characteristic of the intracellular cytoplasm.

11.2 Solutions to the Diffusion Equation

Before we discuss the impulse response or Green's function of the diffusion equation, let us sketch out its macroscopic phenomenological derivation. The mathematical theory of diffusion in an isotropic milieu is based on the simplest phenomenological expression possible—also called Fick's first law of diffusion (Fick, 1855)—that the rate of transfer $S(x, t)$ of a diffusing substance across a surface of unit area (also called the flux; Eq. 9.2) is proportional to the concentration gradient measured normal to the surface,

$$S(x, t) = -D\frac{\partial C(x, t)}{\partial x} \tag{11.14}$$

TABLE 11.1
Diffusion Coefficients

Ion or molecule	Diffusion coefficient
H^+	9.3[1]
NO	3.8[2]
Na^+	1.33[1]
K^+	1.96[1]
Ca^{2+}	0.6[3]
IP_3	0.2[4]
Calmodulin	0.13
CaM kinase II	0.034

Diffusion coefficients in an aqueous environment for different ions and second messenger molecules in units of 10^{-5} cm^2/sec, that is $\mu m^2/msec$.
[1] Table 10.1 in Hille (1992).
[2] In rat cortex; Meulemans (1994); see also Wise and Houghton (1968).
[3] Blaustein and Hodgkin (1969).
[4] Allbritton, Meyer, and Stryer (1992).

where D is the constant of proportionality and the minus sign arises because diffusion occurs against a concentration increase. Since the amount of substance diffusing across the boundary is proportional to the area of the boundary, the diffusion coefficient has dimensions of $\mu m^2/msec$.

Because this amount corresponds to a particular number of molecules diffusing, we refer to it using the colloquial, but entirely appropriate, term *stuff* for lack of a more specific term and express it in units of gram molecules or moles (mol) while the concentration C is given in molars (M), that is moles of molecules per liter.[1] The extracellular concentration of Ca^{2+} ions is about 2 mM, while its intracellular concentration at rest is around 10 to 20 nM, a difference of five orders of magnitude.

Consider a cylindrical cable where the concentration C only varies along the x dimension, reducing the problem of solving the diffusion equation from three dimensions to one. The justification of this is identical to the one we made for one-dimensional cable theory in Chap. 2, namely, that the radius of the cylinder is much shorter than its length and that the equilibrium time for radial diffusion is short compared to longitudinal diffusion.

If the concentration inside a compartment centered at x and with boundaries at $x+\Delta x$ and $x-\Delta x$ (Fig. 11.2) varies by $\partial C/\partial t$, the change in the amount of stuff in this compartment is given by

$$\frac{\Delta x \pi d^2}{2} \frac{\partial C(x,t)}{\partial t}. \tag{11.15}$$

This change should be identical to the net rate of transfer across one boundary minus the rate of transfer across the other,

$$\frac{\pi d^2}{4}(S(x-\Delta x,t) - S(x+\Delta x,t)). \tag{11.16}$$

Setting these two expressions equal leads to

$$\frac{\partial C(x,t)}{\partial t} = \frac{S(x-\Delta x,t) - S(x+\Delta x,t)}{2\Delta x}. \tag{11.17}$$

In the limit of an infinitesimally small interval ($\Delta x \to 0$), the expression $S(x+\Delta x,t) - S(x-\Delta x,t)$ converges to $2\Delta x\, \partial S(x,t)/\partial x$. Applying Eq. 11.14 we arrive once again at the *diffusion equation*

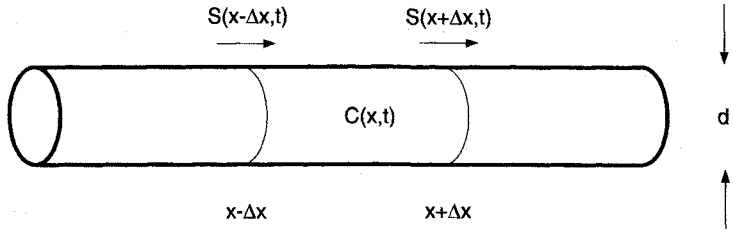

Fig. 11.2 DIFFUSION IN A CYLINDER Diffusion of some substance into and out of a cylindrical compartment with boundaries at $x-\Delta x$ and $x+\Delta x$. $S(x,t)$ corresponds to the rate of transfer across the cross section of area $\pi d^2/4$, and $C(x,t)$ corresponds to the concentration. As in one-dimensional cable theory, under certain conditions the three-dimensional diffusion equation can be reduced to a one-dimensional one.

1. To remind the reader, one mole of water, that is, 18 grams molecules, corresponds to 6.023×10^{23} H_2O molecules. Its concentration is 1000 grams per liter divided by 18 grams per mole, that is 55 M.

$$\frac{\partial C(x,t)}{\partial t} = D\frac{\partial^2 C(x,t)}{\partial x^2}. \tag{11.18}$$

This is a linear partial differential equation of the parabolic type, with a unique solution if both an initial and a boundary condition are specified. We wish to point out already here, although we will not exploit this similarity until Sec. 11.7, that Eq. 11.18 is isomorphic to the linear cable equation (Eq. 2.7) if $r_m \to \infty$ (Fig. 11.3).

11.2.1 Steady-State Solution for an Infinite Cable

What is the steady-state behavior of the diffusion equation? If, in analogy with the cable equation, we "clamp" the concentration at the origin $C(x = 0, t)$ for all times to a fixed value C_0, Eq. 11.18 reduces to an ordinary differential equation,

$$\frac{d^2 C(x)}{dx^2} = 0. \tag{11.19}$$

Its solution for an infinite cable is $C(x) = C_0$ for all values of x. After enough time has passed, the concentration in the entire cable rises to the concentration at the origin. This behavior is in marked contrast to the exponential decay of the potential in response to a current step (Eq. 2.12) and is a consequence of the fact that none of the diffusing substance "leaks" out across the walls of the cylinder.

11.2.2 Time-Dependent Solution for an Infinite Cable

The simplest time-dependent solution is the one for the concentration change along an infinite one-dimensional cable if an amout S_0 of calcium ions is injected instantaneously

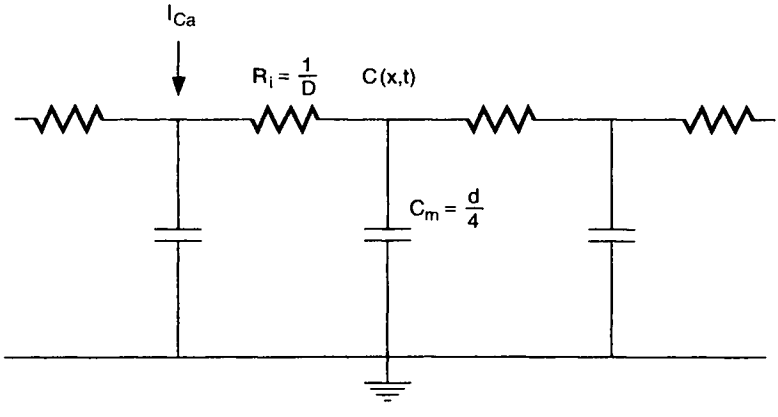

Fig. 11.3 Equivalent Electrical Circuit Associated with the Diffusion Equation Lumped electrical circuit representation associated with the diffusion of a substance in an elongated fiber. The input here is defined as $2I_{Ca}/Fd$, where d is the diameter of the process, F is Faraday's constant, and I_{Ca} is the calcium current flowing across the membrane. With the membrane capacity c_m set to 1 and $r_a = 1/D$, this circuit can be mapped onto the lumped electrical circuit approximating the cable equation (Fig. 2.3) in the absence of any membrane conductance (that is, $r_m \to \infty$). As we will show in Sec. 11.7, this analogy to the cable equation can be extended to the presence of a fast buffer and ionic pumps in the membrane. In the limit of infinitely small mesh size, the solution to this circuit approximates the continuous diffusion equation (Eq. 11.18).

into the cylinder at $x = 0$. We can show by simple differentiation that the resulting spatio-temporal evolution of C is given by

$$C_\delta(x,t) = \frac{S_0}{\sqrt{2\pi}} \frac{1}{(2Dt)^{1/2}} e^{-\frac{x^2}{4Dt}} . \tag{11.20}$$

The associated concentration profile is plotted in Fig. 11.4 for different values of t and x. In comparing this function with the impulse response function of the infinite, passive cable (Eq. 2.31 and Fig. 2.6), we notice the absence of an e^{-t} term (caused by the lack of a finite, membrane leak conductance for the diffusion equation). As a consequence, the total amount of substance is conserved, $\int C_\delta(x,t)dx = S_0$, at all times t. The absence of this exponential causes the Green's function for the diffusion equation to decay less rapidly than the corresponding Green's function for the cable equation. In particular, and not surprisingly, given our earlier result concerning the variance in the mean position of a cloud of randomly moving particles, the variance of the impulse response function increases linearly with time. We expand upon this point in the following section.

11.2.3 Square-Root Relationship of Diffusion

For any fixed time t, Eq. 11.20 can be expressed as a Gaussian, as can be seen upon inspection of Fig. 11.4A,

$$C_\delta(x,\sigma) = \frac{S_0}{\sigma\sqrt{2\pi}} e^{-\frac{x^2}{2\sigma^2}} \tag{11.21}$$

with

$$\sigma = \sqrt{2Dt} . \tag{11.22}$$

The variance of the Gaussian increases linearly with t, or the standard deviation increases with the square root of time. This has important consequences.

Let us consider the concentration in a semi-infinite cylinder, where the concentration at one end is held fixed: $C(x = 0, t) = C_0$ for all times. In the case of the cable equation, this would be equivalent to clamping the voltage at one end of the cable. We can solve for $C(x,t)$ directly by using either Fourier or Laplace transforms (Crank, 1975),

$$C(x,\sigma) = C_0 \operatorname{erfc}\left(\frac{x}{\sigma\sqrt{2}}\right) \tag{11.23}$$

where $\operatorname{erfc}(x)$ is the complementary error function defined as

$$\operatorname{erfc}(z) = \frac{2}{\sqrt{\pi}} \int_z^{+\infty} e^{-y^2} dy \tag{11.24}$$

with $\operatorname{erfc}(0) = 1$. The propagation of this concentration increase along the cylinder—illustrated in Fig. 11.5—involves only the dimensionless parameter $x/(\sigma\sqrt{2})$. Due to the square-root relationship between σ and t, it follows that the time required for any location to reach a given concentration is proportional to the square of the distance. If we ask at what time $t_{1/2}(x)$ the concentration at x reaches half of the source concentration, that is, $C_0/2$, we solve for t in Eq. 11.23, with its left-hand side set to $C_0/2$. By consulting tables for the error function (such as in Crank, 1975), we see that $\operatorname{erfc}(0.5) \approx 1/2$ within a few percent. In other words, $x/(2\sqrt{Dt_{1/2}}) \approx 1/2$, or

$$t_{1/2} \approx \frac{x^2}{D} . \tag{11.25}$$

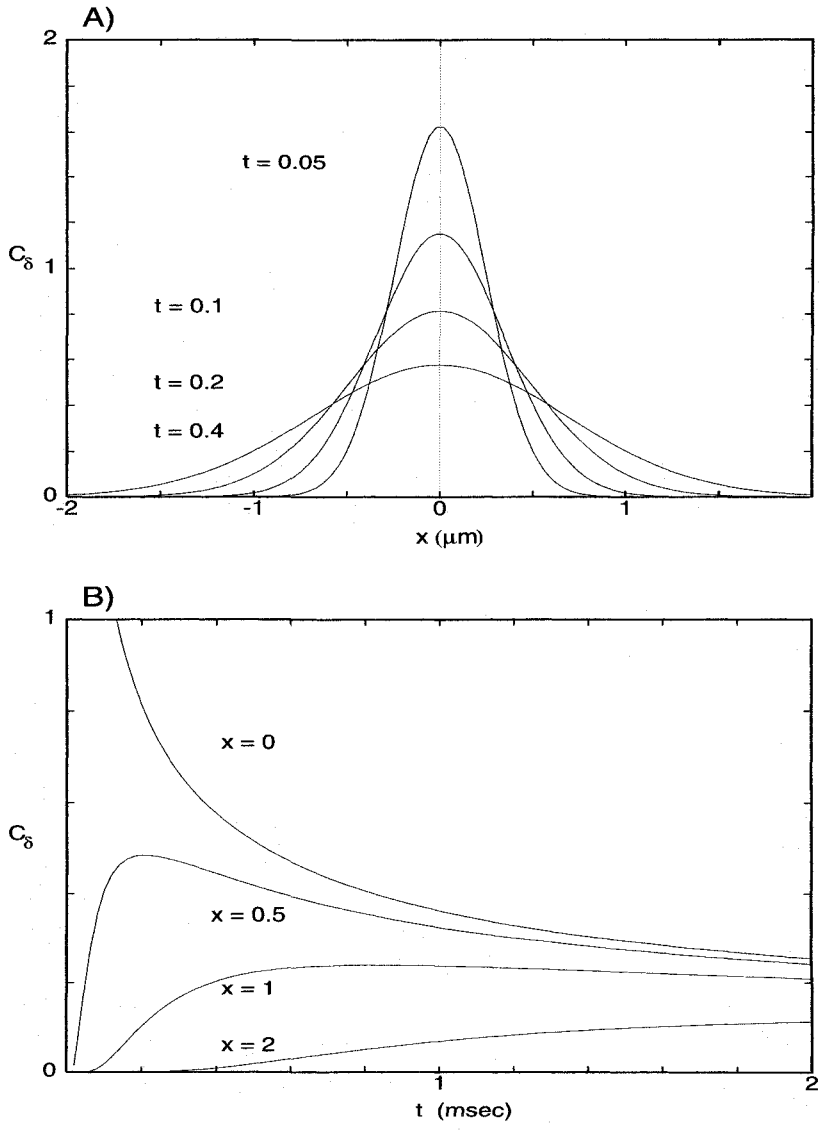

Fig. 11.4 Impulse Response of the Diffusion Equation in an Infinite Cable Concentration $C_\delta(x, t)$ in an infinite cylinder in response to an instantaneous injection of substance at $t = 0$ at the origin $x = 0$ as a function of space (**A**) or time (**B**; see Eq. 11.20). This Green's function decays more slowly than the Green's function of the linear cable equation (Eq. 2.31). As is clear from panel **A**, for any fixed time t the impulse response function can be described as a Gaussian, whose variance increases linearly with time.

Note that the approximation only involves the numerical factor in front of the square. We can reformulate this equation by stating that for a given duration t from the onset of the concentration step, the distance $x_{1/2}$ at which the concentration has reached half of its peak value is given by

$$x_{1/2} \approx \sqrt{Dt}\,. \tag{11.26}$$

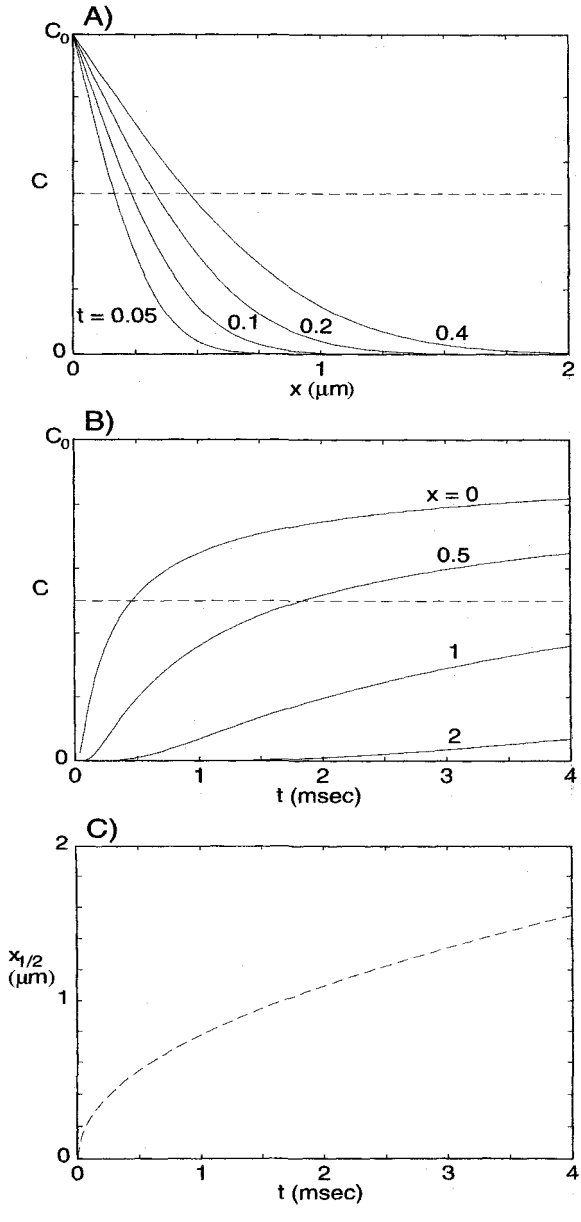

Fig. 11.5 THE SQUARE-ROOT LAW OF DIFFUSION At $t = 0$, the calcium concentration at the origin of a semi-infinite cable is clamped to C_0. **(A)** Evolving concentration profile along the cable. **(B)** As time goes by, the concentration throughout the cable slowly rises to C_0 (different from the solution of the cable equation). At any one instance, we can ask at what location $x_{1/2}$ along the cable the concentration first reaches $C_0/2$ (dashed line). This relationship, shown in **(C)**, is a square-root one. It takes four times as long to diffuse twice the distance (Eq. 11.26). This imposes a fundamental physical constraint on how fast any substance can diffuse in one or more spatial dimensions.

In three-dimensional space, the right-hand side needs to be multiplied by $\sqrt{3}$ (as in Eq. 11.12). If considering diffusion of ions within the porous and highly restricted extracellular space, further adjustments are necessary (see Sec. 20.2).

As an example, let us assume that the concentration of calcium at one end of a one-dimensional cylinder is clamped to 1 μM. Assuming that no buffer impedes the diffusion of the calcium ions along the cable (and that $D_{Ca} = 0.6\ \mu m^2/msec$), a calcium front—defined here as the time at which the concentration at any one location first reaches 0.5 μM—moving down the cylinder takes about 1 msec to cover the first 0.77 μm, 10 msec to propagate

2.5 μm away from the origin and has traveled only 7.7 μm after 100 msec (Fig. 11.5). In neuronal tissues, these times are considerably further reduced due to the binding of calcium to intracellular buffers (Sec. 11.4).

The linear diffusion equation, as a member of the family of parabolic differential equations which also includes the linear cable equation (Sec. 2.3), does not admit to any solution $C(x, t) = C(x - vt)$ that propagates with fixed velocity v along the cable. This behavior is in stark contrast to the linear relationship between distance and time for action potentials propagating down the axon or for the wave of calcium release occurring in eggs following fertilization, making the cells impervious to the entry of additional sperms.

The square-root behavior imposes a fundamental limitation on the time required for concentration changes of calcium or any other intracellular messenger to affect distant sites (in the absence of active transport systems) and is apparent everywhere. For instance, if we keep the concentration of calcium in the shell just below the membrane of a spherical cell constant, the center of the sphere will have reached one half the shell concentration after about $0.04d^2/D$ msec, where d is the diameter of the sphere (in micrometers). For additional solutions to the diffusion equation under various boundary conditions consult Crank (1975) and the monograph by Cussler (1984).

11.3 Electrodiffusion and the Nernst-Planck Equation

In the derivation of the cable equation in the second chapter, we had assumed that the concentration of ions does not vary along the longitudinal direction of the cable. Thus, ions are only propelled along the cable by the voltage gradient, giving rise to the $\partial^2 V/\partial x^2$ term. In the previous section, we discussed the effective motion of ions due to diffusion, down the concentration gradient.

In general, of course, we need to include the movement of ions caused by concentration differences as well as by drift along the electric field. Even if a dendrite is initially at equilibrium with respect to the spatial distribution of sodium, potassium, calcium, and chloride ions, which are most important for fast signaling, the influx and efflux of ions across the membrane disturb this equilibrium. This is particularly true for very small volumes, such as thin dendrites or spines where the influx of even a moderate amount of calcium significantly increases $[Ca^{2+}]_i$, creating concentration gradients that propel calcium ions down this gradient (in addition to any existing voltage gradient).

In order to account for these effects, we need to combine Fick's law (Eq. 11.14) with Ohm's law, something done by Nernst (1888, 1889) as well as Planck (1890). Assuming that the longitudinal current and ionic concentrations are uniform across the cross section of the cylindrical dendrite or axon and that the random, diffusional motion superimposes linearly onto the electrotonic motions of ions driven by a true "force," we can write the one-dimensional *Nernst-Planck electrodiffusion equation* (Hille, 1992),

$$I_{i,k}(x, t) = -z_k F D_k \frac{\partial C_k(x, t)}{\partial x} - \frac{z_k^2 F^2 D_k C_k(x, t)}{RT} \frac{\partial V_m(x, t)}{\partial x} \tag{11.27}$$

where $I_{i,k}(x, t)$ is the axial current for the ionic species being considered (here labeled k), z_k is its valence, D_k its diffusion coefficient, R the gas constant, and F Faraday's constant.

The $z_k F D_k$ term in front of the concentration gradient converts "stuff" into a current, while the constants in front of the potential gradient express implicitly how the electrical conductance relates to the concentration and the mobility of the ions (see also Eq. 11.13).

Thus, ions drift down the potential gradient, while simultaneously spreading due to diffusion. Hodgkin has remarked that while diffusion is like a hopping flea, electrodiffusion is like a flee that is hopping in a breeze.

As an aside, let us note that application of this kinetic equation in the direction perpendicular to the membrane directly yields Eq. 4.3 for the synaptic reversal or Nernst potential of an ionic current at equilibrium. Since the net current across the membrane must be zero, we can rearrange Eq. 11.27,

$$\frac{dV_m(r)}{dr} = -\frac{RT}{z_k F}\frac{1}{C_k(r)}\frac{dC_k(r)}{dr} = -\frac{RT}{z_k F}\frac{d}{dr}\log C_k(r) \tag{11.28}$$

with r the spatial variable across the membrane. Integrating this across the membrane yields the expression for the Nernst potential associated with each ionic species k.

Let us return to our main argument. Due to reasons of conservation, the change in concentration of the ions in an infinitesimally small cylindrical segment of length δx and diameter d must be balanced by the sum of the transmembrane current $i_{m,k}(x,t)$ per unit length (suitably weighted by the surface-to-volume ratio $4/d$; Fig. 11.2) and the difference between the ingoing and outgoing axial currents, or

$$\frac{4}{d} i_{m,k}(x,t) + \frac{\partial I_{i,k}(x,t)}{\partial x} + z_k F \frac{\partial C_k(x,t)}{\partial t} = 0. \tag{11.29}$$

Taking the spatial derivative of both sides of the electrodiffusion equation and extracting the expression for the change in concentration from Eq. 11.29 leads to

$$\frac{\partial C_k(x,t)}{\partial t} = -\frac{4}{z_k F d} i_{m,k}(x,t) + D_k \frac{\partial^2 C_k(x,t)}{\partial x^2} + \frac{z_k F D_k}{RT}\frac{\partial}{\partial x}\left(C_k(x,t)\frac{\partial V_m(x,t)}{\partial x}\right). \tag{11.30}$$

The terms on the right-hand side of this nonlinear coupled partial equation correspond to the transmembrane current (given either by Ohm's law with the appropriate reversal potential or by the GHK current equation), the familiar diffusional term, and a voltage gradient term. In general, this equation must be solved for each species of ions that is present at relevant concentrations (assuming that different ionic species move independent of each other, something that may not always be true).

Since Eq. 11.30 is a single equation in two unknowns $C_k(x,t)$ and $V_m(x,t)$, it needs to be supplemented by an equation specifying the membrane potential, here expressing the fact that $V_m(t)$ is determined by the change in the total charge—added over all ionic species k weighted by their valence—divided by the membrane capacitance C_m in addition to an offset term, or

$$V_m(x,t) = V_{\text{rest}} + \frac{Fd}{4C_m}\sum_k z_k \left(C_k(x,t) - C_{k,\text{rest}}\right) \tag{11.31}$$

where $C_{k,\text{rest}}$ is the resting concentration of the kth ionic species.

In principle we need to solve Eqs. 11.30 and 11.31 to describe the dynamics of the membrane potential in extended cable structures properly (supplemented by an additional constraint at branching points; Qian and Sejnowski, 1989). However, this does not come cheaply. When linearly coupling two differential equations, the temporal discretization step

Δt required for an accurate evolution of the system is, in general, the smaller of the two time steps associated with the individual equations. In other words, the discretization necessary to solve Eq. 11.27 has to be much finer in both time and space than the discretization required for solving the cable equation with constant concentrations, resulting in much longer running times for the numerical algorithm.

11.3.1 Relationship between the Electrodiffusion Equation and the Cable Equation

In "large" neuronal processes, the intracellular concentration of various ions changes by relatively small amounts, implying that the diffusional contributions are negligible and that the longitudinal currents are purely resistive. It is straightforward to obtain the familiar cable equation as a special case of Eq. 11.30 by assuming that the axial ionic concentration gradients can be neglected, $\partial C_k(x,t)/\partial x \approx 0$. In combination with Eq. 11.29, Eq. 11.30 reduces to

$$C_m \frac{\partial V_m}{\partial t} + \sum_k i_{m,k}(x,t) = \frac{d}{4}\frac{F^2}{RT}\sum_k D_k z_k^2 C_k \frac{\partial^2 V_m}{\partial x^2}. \tag{11.32}$$

This corresponds to the cable equation if we identify the intracellular resistance R_i with

$$R_i = \frac{RT}{F^2}\frac{1}{\sum_k D_k z_k^2 C_k}. \tag{11.33}$$

Qian and Sejnowski (1989) compare numerical simulations of the propagating action potential in the squid giant axon (with a 0.476 mm diameter) using the electrodiffusion equation against the cable model solution of Cooley and Dodge (1966). With the diffusion coefficients for sodium and potassium reported in Table 11.1, they calculate R_i from Eq. 11.33, obtaining 33.4 Ω·cm for the potassium resistance and 267 Ω·cm for the sodium resistance, for a total value of $R_i = 29.7$ Ω·cm. This last value is reasonably close to the internal resistance of 35.4 Ω·cm used by Hodgkin and Huxley (1952d). The final solutions are indistinguishable from those of Cooley and Dodge (1966). Reducing the diameter several hundredfold to 1 μm only leads to a maximum relative concentration change of 1.4%, too small to have any significant effect. Thus, as in a metal wire, charged carriers[2] move under the influence of Ohm's law and diffusion does not play any (significant) role.

The concentration change due to synaptic input scales as $1/r$, implying that for submicrometer dimensions, diffusional transport of ions will contribute substantially to the total current. Chapter 12 deals with one such case, dendritic spines, where a single excitatory or inhibitory synaptic input can change the concentration of calcium or chloride significantly on a very rapid time scale. Here the predictions of the electrodiffusion model can deviate substantially from those of the cable model.

11.3.2 An Approximation to the Electrodiffusion Equation

From a physical point of view, the electrodiffusion equation constitutes a better description of current flow in a neuronal process than the cable equation. Thus, it behooves us to routinely use the former, rather than the latter, for simulating events in dendrites. Yet, because of the additional computational load imposed by solving Eq. 11.30 using a finer spatiotemporal discretization grid than the one required for solving the cable equation, almost

2. Electrons in one case and Na^+, K^+, and other ions in the other.

nobody has done this. Qian and Sejnowski (1989) offer a remedy for this by describing a fast approximation for solving the electrodiffusion equation in extended cable structures. It involves replacing the constant intracellular resistance R_i by batteries and resistances for each ionic species being considered (Fig. 11.6). At each time step, this algorithm

1. Calculates the intracellular concentration of each ionic species in each compartment by integrating over both the transmembrane and the intraaxial currents between compartments.
2. Computes the new value of the Nernst reversal potential for each ionic species for each compartment across the membrane (E_{Na} and E_K in Fig. 11.6).
3. Replaces the single intracellular resistance R_i of the cable equation with individual longitudinal resistances,

$$R_{i,k} = \frac{RT}{F^2} \frac{1}{D_k z_k^2 C_k} \tag{11.34}$$

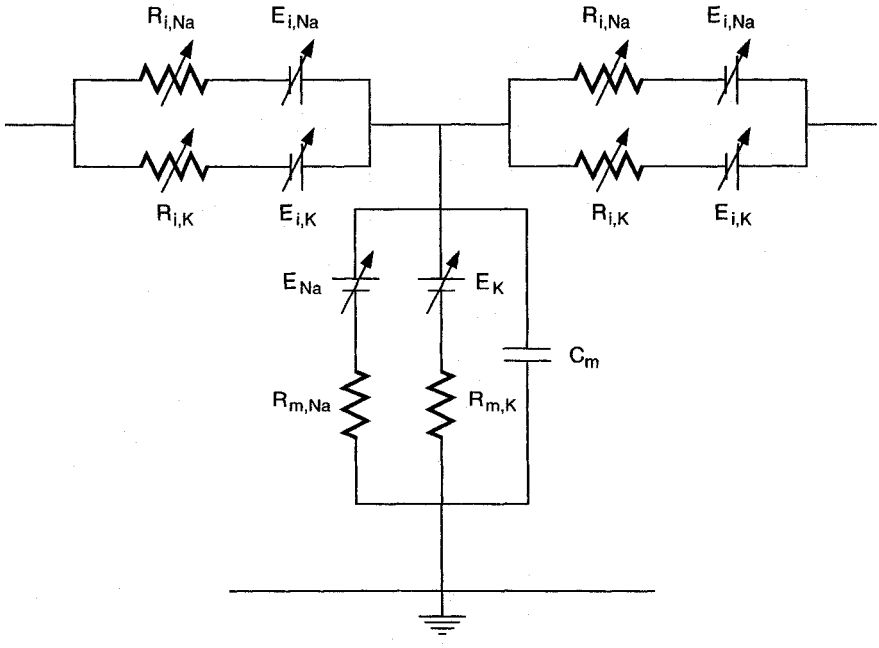

Fig. 11.6 Approximating the Electrodiffusion Equation Solving the electrodiffusion equation, a better description of the transport of charged ions than the cable equation, is computationally more demanding than solving the cable equation (due to the higher spatial and temporal discretization required). Qian and Sejnowski (1989) advocate the usage of an approximation to Eq. 11.30, illustrated here. The crucial step is to replace (at each time step and for each compartment) the single axial resistance R_i of the cable equation (Fig. 2.3) with a resistance $R_{i,k}$ and battery $E_{i,k}$ for each ionic species being considered. The transmembrane reversal batteries E_{Na} and E_K are given by the Nernst equation (Eq. 4.3). This procedure is illustrated for the thick squid giant axon using a symmetrical discretization procedure with $R_{i,Na} = 267\ \Omega\cdot$cm and $R_{i,K} = 33.4\ \Omega\cdot$cm. Given the tiny changes in intracellular sodium and potassium concentration, $E_{i,Na} \approx E_{i,K} \approx 0$. Even for a much thinner axon of 1 μm-diameter, the maximal value of these batteries is 0.4 mV. Only for very thin distal dendrites or spines will qualitative differences to the cable model appear. Reprinted in modified form by permission from Qian and Sejnowski (1989).

and batteries between compartment j and $j + 1$,

$$E_{i,k} = \frac{RT}{Fz_k} \log \frac{C_k(j)}{C_k(j+1)} \tag{11.35}$$

for each ionic species k.

For most situations that Qian and Sejnowski considered, this algorithm agrees well with the solutions to the full electrodiffusion equation, only doubling execution times in comparison to solving the cable equation. When in doubt whether or not diffusion of ions will affect the solution of the cable equation, we would recommend this algorithm to the reader (for more details, see Qian and Sejnowski, 1989).

11.4 Buffering of Calcium

In a classical experiment, Hodgkin and Keynes (1957) used radioactive ^{45}Ca to track the diffusion of calcium in squid axon fibers. From the observed broadening of the radioactive patches the effective diffusion constant was estimated to be about one-tenth of the diffusion coefficient D_{Ca} in aqueous solution. This is in contrast to the behavior of potassium ions under similar circumstances. This showed that once calcium enters the intracellular cytoplasm it is not free to diffuse. Indeed, 95% and more of the entering calcium is quickly bound by a host of systems, ranging from a set of different protein buffers to cellular organelles, such as mitochondria and the smooth endoplasmic reticulum. Mitochondria have a considerable ability to accumulate (and release) Ca^{2+}. The endoplasmic reticulum in neurons—related to the sarcoplasmic reticulum in skeletal muscle cells, which is responsible for the release and subsequent reuptake of Ca^{2+} during muscle contractions—also accumulates calcium, yet at a relatively slow rate. Since the calcium uptake of these organelles takes place on a time scale of seconds and longer (Rasgado-Flores and Blaustein, 1987), we focus our discussion on the dynamics of calcium binding to protein buffers. (For an overview of neuronal calcium homeostasis, see Carafoli, 1987; McBurney and Neering, 1987; Blaustein, 1988; Clapham, 1995.)

A large number of Ca^{2+}-binding proteins, such as calmodulin, calbindin, and parvalbumin, are present at high concentrations in nerve cells. The most important neuronal calcium buffer, *calmodulin*, a 15,000 dalton regulatory protein, is present in brain tissue at a concentration of 30–50 μM and acts as an internal *calcium sensor* (Manalan and Klee, 1984; see Fig. 11.7). It is located in the cell bodies, dendrites, and postsynaptic densities of most neurons in the central nervous system, but not in axons. Each calmodulin (CaM) molecule has four Ca^{2+}-binding sites. At resting levels of calcium concentration, none or only one of these sites is occupied. As the concentration of free calcium rises to micromolar levels, the four binding sites are occupied successively. The fully bound calcium-calmodulin complex in turn can bind to a large number of regulatory proteins to alter their function, such as calmodulin-dependent protein kinases (CaM kinases), protein phosphatases, and adenylate cyclases.

These enzymes, some of which have been implicated in the induction of long-term potentiation (Miller and Kennedy, 1986; Kennedy, 1989, 1992; Ghosh and Greenberg, 1995), can trigger the modification of other synaptic proteins locally at the synapse or can mediate more general cellular responses by activating molecules involved in the regulation of gene expression. As the concentration of calcium in the cytoplasm drops, the calcium ions are progressively released from the buffer and are free to wander about. The resulting

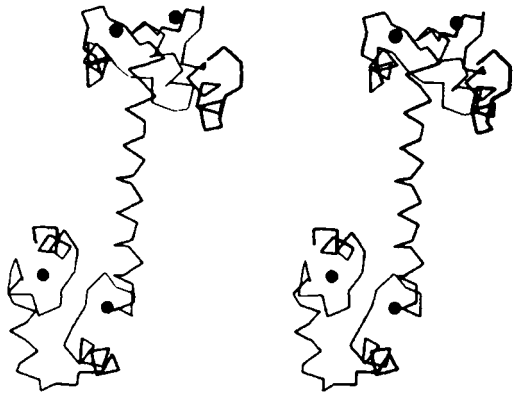

Fig. 11.7 STRUCTURE OF CALMODULIN Calmodulin is the most important calcium receptor protein. It is ubiquitous in eukaryotic cells and is found in the brain at concentrations of 30–50 μM. The 15,000-dalton protein can bind four Ca^{2+} ions in a cooperative manner with dissociation constants in the μM range. In the absence of calcium, the protein has some structure. Binding of Ca^{2+} to all four sites induces a conformational change, leading to a dumbbell-shaped molecule. Two heads, each of which contains the two bound calcium ions, are interconnected by a long α chain. In this form, the calcium-calmodulin complex can interact with a large number of other proteins, giving rise to a complex regulatory network. Reprinted by permission from Babu et al., (1985).

changes, which were triggered by the initial binding of Ca^{2+} ions to calmodulin, can outlast, by far, the calcium transient (Sec. 20.1). Before we come to this, let us first quantify the dynamics of various types of binding.

11.4.1 Second-Order Buffering

In one of the simplest chemical reactions possible, a single calcium ion binds to a single buffer molecule B, resulting in a bound buffer-calcium complex B·Ca. If the *forward binding rate* with which this reaction proceeds is f (in units of bindings per second per molar) and the *backward rate* is b (in units of bindings per second), we have

$$B + Ca^{2+} \rightleftharpoons B \cdot Ca . \tag{11.36}$$

In terms of associated kinetic equations, we can write

$$\begin{aligned} \frac{d[Ca^{2+}]}{dt} &= b[B \cdot Ca] - f[B][Ca^{2+}] \\ \frac{d[B]}{dt} &= b[B \cdot Ca] - f[B][Ca^{2+}] \\ T_B &= [B \cdot Ca] + [B] \end{aligned} \tag{11.37}$$

where [B] and [B·Ca] denote the concentrations of the buffer and the buffer-calcium complex. The last equation expresses the fact that only a fixed amount T_B of buffer molecules exists, where T_B corresponds to the total amount of the buffer. f and b tell us something about the speed with which the buffering reaction occurs. The above type of reaction is known as a *second-order reaction*, since two substances participate, each with 1 mol, resulting in a quadratic term in the associated kinetic Eq. (11.37) (Pauling and Pauling, 1975).

Setting the temporal derivative to zero yields the steady-state distribution of the buffer-calcium complex,

$$[\mathrm{B}\cdot\mathrm{Ca}] = \frac{T_\mathrm{B}[\mathrm{Ca}^{2+}]}{K_d + [\mathrm{Ca}^{2+}]} \tag{11.38}$$

where $K_d = b/f$ is the *dissociation constant* of the buffer expressed in molars. If the calcium concentration has reached K_d, exactly half the available buffer is bound to calcium. The lower K_d, the lower the calcium concentration at which the buffer begins to bind Ca^{2+} ions. K_d therefore tells us something about the *affinity* of the buffer. The K_d of most calcium binding proteins is in the low to mid micromolar range.

If the calcium concentration is much less than K_d, Eq. 11.38 can be approximated by

$$[\mathrm{B}\cdot\mathrm{Ca}] \approx [\mathrm{Ca}^{2+}]\frac{T_\mathrm{B}}{K_d}. \tag{11.39}$$

At these low calcium concentrations $[\mathrm{B}\cdot\mathrm{Ca}]$ is proportional to $[\mathrm{Ca}^{2+}]$. We will explore the consequences of this in Sec. 11.7.

For $[\mathrm{Ca}^{2+}] < K_d$, the Ca^{2+} *binding ratio*, that is the ratio of bound calcium to free calcium, is given by

$$\beta = \frac{[\mathrm{B}\cdot\mathrm{Ca}]}{[\mathrm{Ca}^{2+}]} = \frac{T_\mathrm{B}}{K_d}. \tag{11.40}$$

This number is usually large, upward of 20 (Allbritton, Meyer, and Stryer, 1992; Neher, 1995; Gabso, Neher, and Spira, 1997), implying that 95% or more of all calcium is bound to intracellular buffers. Clearly the cell cares a great deal about regulating the amount of free calcium ions sloshing around the neuron.

11.4.2 Higher Order Buffering

As mentioned above, the ubiquitous calcium buffer protein calmodulin has four calcium binding sites on each molecule. A general four-site system is defined by more than a dozen rate constants. In particular, binding calcium to one site can induce a conformational change of the molecule, affecting the binding of calcium to the remaining sites. Calmodulin appears to display positive *cooperativity*, such that binding of calcium to the first two binding sites increases the affinity for the remaining two sites. Furthermore, the binding constants for the four sites differ significantly from each other. For the sake of simplicity, we will assume that all four sites are independent of each other and have identical binding constants. The K_d of calmodulin is on the order of 10 μM (Manalan and Klee, 1984; Klee, 1988), such that at 40–50 μM levels of Ca^{2+}, most of the calcium-binding sites will be occupied. For n binding sites, we can write down a series of n second-order equations of the from

$$\mathrm{B}\cdot\mathrm{Ca}_{m-1} + \mathrm{Ca}^{2+} \rightleftharpoons \mathrm{B}\cdot\mathrm{Ca}_m \tag{11.41}$$

with $m = 1, 2, \cdots, n$. By repetitively applying the associated kinetic equations, we can express the steady-state concentration of all intermediate species and of the fully bound buffer-calcium complex as

$$[\mathrm{B}\cdot\mathrm{Ca}_n] = T_\mathrm{B}\frac{([\mathrm{Ca}^{2+}]/K_d)^n}{1 + \sum_{m=1}^{n}([\mathrm{Ca}^{2+}]/K_d)^m} \tag{11.42}$$

where T_B is the total concentration of the buffer in its various guises.

In the case of calmodulin, the forward rate constant f is about 50 per second and per micromolar, the backward rate b is about 500 per second, implying a dissociation constant

$K_d = 10\,\mu M$. Therefore, as long as $[Ca^{2+}]$ is less than a few micromolar, the denominator in Eq. 11.42 is close to 1 and the steady-state concentration of the fully bound calmodulin complex will be proportional to the fourth power of calcium. Each additional binding step to another protein or enzyme will potentiate or sharpen the polynomial relationship between $[Ca^{2+}]$ and the buffer, since n increases by 1 in the above equation.

Computationally, higher order binding processes can be thought of as a squaring (for $n = 2$) or an nth-order polynomial operation (Koch and Poggio, 1992). Gamble and Koch (1987) showed numerically that a fast burst of action potentials (10 spikes at 333 Hz) to a synapse located on a spine elevates intracellular calcium in the spine head by about a factor of 5 in comparison to the peak calcium evoked after 10 spikes at 50 Hz (see also Chap. 12). This difference in levels of free calcium in the low- versus high-frequency input situation is amplified 1000-fold if the concentration of fully bound calmodulin is considered; in the first case 1000 times more $[CaM \cdot Ca_4]$ is evoked than in the latter case (roughly about a factor of 5^4). If a certain level of concentration of some critical substance is required to initiate some reaction, multiple binding steps will tend to lead to an all-or-none threshold behavior.

11.5 Reaction-Diffusion Equations

Let us now combine the diffusion equation for calcium with the kinetic equations expressing the binding of calcium to a single buffer via a second-order reaction. We assume that the buffer itself is stationary and does not diffuse and denote the intracellular calcium concentration as $[Ca^{2+}](x, t)$. The equations governing the evolution of the calcium and the bound buffer concentration, frequently referred to as *reaction-diffusion* equations, are of the form

$$\begin{aligned} \frac{\partial [Ca^{2+}](x,t)}{\partial t} &= D\frac{\partial^2 [Ca^{2+}](x,t)}{\partial x^2} - \frac{\partial [B \cdot Ca](x,t)}{\partial t} \\ \frac{\partial [B \cdot Ca](x,t)}{\partial t} &= f[B](x,t)[Ca^{2+}](x,t) - b[B \cdot Ca](x,t) \\ T_B &= [B \cdot Ca] + [B] \end{aligned} \tag{11.43}$$

As the reader can see, these coupled partial differential equations are nonlinear, due to the fact that we assumed cooperative binding between calcium and buffer (expressed in the $[B] \cdot [Ca^{2+}] = (T_B - [B \cdot Ca]) \times [Ca^{2+}]$ term), making their analytical solution difficult (Chap. 14 in Crank, 1975, catalogues the major known solutions). If additional buffers are included or calcium binds to calmodulin or other proteins with multiple binding sites, further equations are required.

Coupled reaction-diffusion equations are well known in developmental biology. They were first invoked by the computer science pioneer Turing (1952) to explain the regular structures in biological systems and have been used to explain the stripes of the zebra and of certain fish (Kondo and Asai, 1995) and aspects of embryonic development in frogs and fruit flies (Kauffman, 1993; Meinhardt, 1994).

A particularly simple and insightful solution to Eq. 11.43 can be obtained if the concentration of the buffer-calcium complex is proportional to the concentration of calcium. This occurs if the binding of calcium to the buffer is very fast compared to the time scale of diffusion *and* if the calcium concentration is much less than the K_d of the buffer (*instantaneous buffer model*).

The first condition implies that the buffer is always at equilibrium relative to the diffusional time scale, while the second condition implies that $[B \cdot Ca] = \beta[Ca^{2+}]$ (Eq. 11.39, where β is defined in Eq. 11.40). Both assumptions allow us to reduce the nonlinear reaction-diffusions Eqs. 11.43 to a single linear equation with

$$\frac{\partial[Ca^{2+}](x,t)}{\partial t} = D\frac{\partial^2[Ca^{2+}](x,t)}{\partial x^2} - \beta\frac{\partial[Ca^{2+}](x,t)}{\partial t} \tag{11.44}$$

and, therefore,

$$\frac{\partial[Ca^{2+}](x,t)}{\partial t} = \frac{D}{1+\beta}\frac{\partial^2[Ca^{2+}](x,t)}{\partial x^2}. \tag{11.45}$$

In other words, in the presence of fast buffering dynamics and relatively small amounts of calcium, the spatio-temporal dynamics of calcium ions are governed by the canonical diffusion equation, except that the original diffusion coefficient is replaced by a smaller one,

$$D_{\text{eff}} = \frac{D}{1+\beta} = \frac{D}{1+T_B/K_d}. \tag{11.46}$$

Diffusion is slowed down, since the Ca^{2+} ions bind to the buffer and are therefore not available to diffuse. In the case of intracellular cytoplasm containing calmodulin at $T_B = 100\ \mu M$ (with K_d in the 5–10 μM range), the effective diffusion coefficient D_{eff} for calcium is at least 10 times slower than the coefficient measured in aqueous solution, in agreement with the Hodgkin and Keynes (1957) experiment mentioned. Due to the square-root relationship between time and distance, this translates into a substantially reduced ability of calcium to act as a fast intracellular messenger if distances larger than a few micrometers are involved.

We conclude that a nondiffusible buffer will always slow down the diffusive spread of calcium.

11.5.1 Experimental Visualization of Calcium Transients in Diffusion-Buffered Systems

One system where the observed calcium dynamics have been compared with numerical calculations are bullfrog sympathetic ganglion cells. These relatively large, spherical cells devoid of dendrites (described in Sec. 9.5) are an ideal test bed for applying confocal laser-scanned microscopy to record the dynamics of intracellular calcium using the fluorescent Ca^{2+} indicator fluo-3. In a pioneering application of this technology, Hernández-Cruz, Sala, and Adams (1990) measured $[Ca^{2+}]_i$ in these cells after application of a voltage-clamp pulse to briefly activate voltage-dependent calcium channels. Because of tradeoffs between temporal and spatial resolution of this method, they recorded the free calcium concentration across a narrow one-dimensional slot that extends across the width of the cell, thereby achieving a 5 msec temporal resolution (Fig. 11.8).

The influx of calcium across the membrane leads to a wave of calcium (Fig. 11.8A and E). Although much of this calcium becomes bound to the resident buffers as well as to the calcium indicator dye, enough remains for the calcium wave to reach the center of the cell after about 300 msec. $[Ca^{2+}]_i$ then equilibrates across the cell (Fig. 11.8F, G, and H), slowly returning to its resting state after 6–8 sec. These basic features were qualitatively reproduced by a radial reaction-diffusion model (Sala and Hernández-Cruz, 1990). It is similar to the model of Yamada, Koch, and Adams (Sec. 9.5) except that it makes no attempt to simulate the voltage dynamics and that it includes *mobile buffers*, that is, buffers that—with or

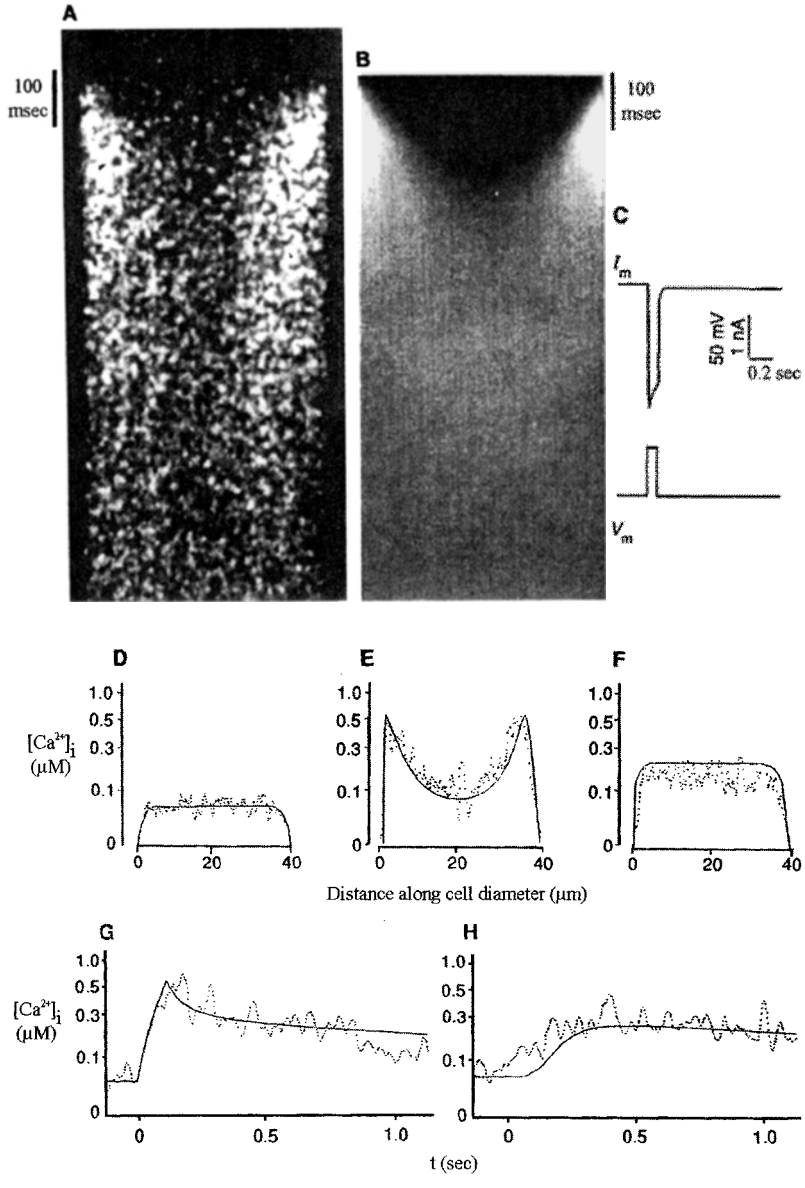

Fig. 11.8 COMPARING EXPERIMENTAL CALCIUM TRANSIENTS AGAINST A MODEL Experimental measurements of intracellular calcium dynamics in bullfrog sympathetic ganglion cells (Hernández-Cruz, Sala, and Adams, 1990) compared to numerical solutions of the associated one-dimensional radial reaction-diffusion equations (Sala and Hernández-Cruz, 1990). The data were obtained by monitoring the calcium dye fluo-3 along a thin strip across the diameter of these spherical cells with the aid of confocal microscopy. Measured (**A**) and simulated (**B**) radial spread of Ca^{2+}. Time extends downward and space across. (**C**) A 100-msec-long voltage-clamp step to +10 mV is used to trigger an influx of Ca^{2+} via voltage-dependent calcium channels (I_m; see also the vertical bars in **A** and **B**). Calcium concentration profiles as a function of space and time extracted from the data in **A** (dotted traces) or the model in **B** (solid traces). (**D**) Resting calcium concentration, $[Ca^{2+}]_i$ is reduced below the membrane due to the presence of calcium pumps in the model. Spatial profile 100 msec (**E**) and 1 sec (**F**) after the stimulus onset. Temporal dynamics of free calcium 2.5 μm below the membrane (**G**) and at the center (**H**) of the 40-μm-diameter cell. Reprinted by permission from Hernández-Cruz, Sala, and Adams, (1990).

without bound calcium—can diffuse inside the cell (with diffusion coefficients of 0.25 and 0.1 μm^2/msec). This causes the decay of calcium below the shell to occur at two different time scales (Fig. 11.8G): a fast one, over within 300 msec, which is due to the diffusional redistribution of Ca^{2+} throughout the cell, and a much slower phase, lasting for seconds, which reflects the slow buffering, the diffusion of the buffer, and the extrusion of calcium across the membrane by the calcium pumps (see the following section).

The qualitative match between observation and model evident in Fig. 11.8 underscores that the evolution of calcium in these simple structures can be understood in terms of diffusion and buffering.

11.6 Ionic Pumps

The crucial component of the system controlling the homeostasis of sodium, potassium, chloride, and calcium are specialized membrane-bound molecules that act as *ionic pumps*. Also known as ion *transporters*, they maintain the ionic gradients across the membrane that enable neurons to signal and to generate and propagate action potentials. In conjunction with buffers and other uptake systems, they also provide exquisite regulation of the intracellular concentration of free Ca^{2+}.

The single most important ion transporter is probably the Na^+–K^+ *pump* (Hille, 1992). It is driven by the energy derived from hydrolysis of ATP. Three Na^+ ions are pumped out of the cell for every two K^+ ions moved into the cell. This results in a net accumulation of charge, that is, in a small but measurable current. The pump is therefore known as *electrogenic* and is ubiquitous in the membranes of all cells, neuronal or not. Given the fact that most cells have stable resting potentials that have to be continuously maintained in the face of EPSPs and IPSPs, action potentials, and so on, the Na^+–K^+ pump consumes a lot of power. Roughly half the metabolic energy used in the retina of a rabbit (Ames et al., 1992) and in the mammalian brain in general (Ames, 1997) has been attributed to it.

Two major transport systems are responsible for the net outward movement of Ca^{2+} across the neuronal membrane against the large concentration gradient (Dipolo and Beauge, 1983; Blaustein, 1988; McBurney and Neering, 1987). One system, the Na^+–Ca^{2+} *exchanger*, exploits the energy gained when moving three Na^+ ions inward by moving one calcium ion out of the cell, thereby generating one excess charge for each Ca^{2+} ion that is removed. This pump has a maximal rate of Ca^{2+} removal of 2–3 nmol per square centimeter of membrane area per second and a K_d in the low micromolar range (that is, the pump is operating at half its maximum if $[Ca^{2+}]_i = K_d$). DiFrancesco and Noble (1985) have developed a model of the cardiac Na^+–Ca^{2+} exchanger, which has also been applied to neurons (Gabbiani, Midtgaard, and Knöpfel, 1994).

A second pump system requires energy in the form of one ATP molecule for each calcium ion pumped out. This ATP-driven calcium pump can be considered to be a pump with a higher affinity ($K_d = 0.2$ μM) yet a lower capacity compared to the Na^+–Ca^{2+} exchanger, with a maximal rate of removal of about 0.2 nmol/cm^2/sec. Its Ca^{2+} dependence is frequently approximated by a Michaelis-Menten equation (see below; Garrahan and Rega, 1990). While both systems operate continuously, the ATP-driven pump can quickly turn on following Ca^{2+} influx subsequent to an action potential, while the lower affinity but much higher capacity system is primarily responsible for maintaining resting levels of Ca^{2+} over longer times.

From the point of view of charge entering or leaving the cell, both ionic pumps have to be treated as ionic currents, the ATP-driven pump acting as an outward current (calcium is removed from the cytoplasm) and the sodium-calcium exchanger acting as an inward current (since three positive charges are moved inside for every two charges being removed). In general, their contributions will be small (but see DeSchutter and Smolen, 1998).

One simple way to model the dynamics of these pumps is via saturable first-order Michaelis-Menten kinetics,

$$\frac{\partial [Ca^{2+}]_{pump}}{\partial t} = \frac{4P_m}{d} \frac{[Ca^{2+}]}{1 + [Ca^{2+}]/K_{d-pump}} \tag{11.47}$$

where P_m is given by the number of calcium ions that can be pumped out per square micrometer of neuronal membrane divided by K_{d-pump}. The $4/d$ factor takes account of the fact that the molecules acting as the pump are inserted into the membrane area (length $\times \pi d$) that encloses the volume (length $\times\ \pi d^2/4$) containing the calcium ions (surface-to-volume ratio). The decrease in calcium concentration due to the action of the pump is directly proportional to the calcium concentration if $[Ca^{2+}] \ll K_d$.

11.7 Analogy between the Cable Equation and the Reaction-Diffusion Equation

As witnessed in previous chapters, a great deal of knowledge and intuition has accumulated about the behavior of the membrane potential in one-dimensional cables and dendritic trees. Can we transfer any of this to the solutions of the reaction-diffusion equations? In particular, can we define appropriate space and time constants to characterize the spatio-temporal dynamics of calcium—or any other substance—in response to synaptic input? Drawing upon the study by Zador and Koch (1994), we show how the techniques developed for one-dimensional cable theory can be applied to reaction-diffusion equations.

Our starting point is the distribution of calcium ions in a cylinder following the influx of a calcium current $I_{Ca}(x, t)$ across the membrane. This current can flow through voltage- or ligand-activated channels. As in one-dimensional cable theory, we neglect the radial components of diffusion, assuming that their associated time constants are much, much faster than the longitudinal ones (e.g., Rall, 1969b).

The inflowing calcium ions diffuse to neighboring locations, bind to various buffers, and can be pumped back out of the cable. The buffer itself can also diffuse with a diffusion coefficient D_B. The expressions governing the resulting change in the concentration of calcium $[Ca^{2+}](x, t)$ and bound calcium-buffer $[B \cdot Ca](x, t)$ is

$$\begin{aligned}
\frac{\partial [Ca^{2+}](x,t)}{\partial t} &= D \frac{\partial^2 [Ca^{2+}](x,t)}{\partial x^2} - f[Ca^{2+}](x,t)[B](x,t) + b[B \cdot Ca](x,t) \\
&\quad - \frac{\partial [Ca^{2+}](x,t)_{pump}}{\partial t} - \frac{2I_{Ca}(x,t)}{Fd} \\
\frac{\partial [B \cdot Ca](x,t)}{\partial t} &= D_B \frac{\partial^2 [B \cdot Ca](x,t)}{\partial x^2} + f[B](x,t)[Ca^{2+}](x,t) \\
&\quad - b[B \cdot Ca](x,t) \\
T_B &= [B \cdot Ca] + [B]
\end{aligned} \tag{11.48}$$

In the first equation, the first term on the right-hand side corresponds to the diffusive contribution to the change in calcium concentration, the second and third terms are caused by the removal of calcium due to its binding with the buffer, the fourth corresponds to the reduction in $[Ca^{2+}]_i$ due to the action of the calcium pump, and the last term converts the inward (that is, negative) calcium current (carrying $2e$ charge per ion) into a calcium concentration (the $4/d$ factor accounts for the area-to-volume ratio). The second equation specifies the change in bound calcium-buffer concentration as a function of diffusion and buffer binding and unbinding. The last equation stipulates that in the absence of any buffer sources and sinks and assuming that the buffer diffuses at the same pace as the bound calcium-buffer complex, the total buffer concentration T_B is constant.

Note the nonlinear coupling between the two variables (the $[Ca^{2+}] \times [B]$ term), rendering the solution to these partial differential equations difficult.

11.7.1 Linearization

As we will show now, under certain limiting conditions, Eqs. 11.48 can be reduced to a *single, linear* partial differential equation, formally equivalent to the cable equation. This reduction is based on the *instantaneous buffer* assumption; that is, the kinetics of buffering are much faster than diffusion. Since the former occurs on a microsecond to millisecond time scale (Falke et al., 1994) and the latter requires 10–100 msec, this is a very valid assumption and implies that

$$f[Ca^{2+}][B] = b[B \cdot Ca] \tag{11.49}$$

holds everywhere.

From a mathematical point of view, Eqs. 11.48 constitute a *singularly perturbed system*, in which one variable evolves much faster than the others. Other instances of such systems are the Hodgkin–Huxley and the FitzHugh–Nagumo equations (Keener, 1988; Wagner and Keizer, 1994). The concentration of the bound buffer at any instant can be approximated by its steady-state distribution (Eq. 11.38),

$$[B \cdot Ca](x,t) = \frac{T_B[Ca^{2+}](x,t)}{K_d + [Ca^{2+}](x,t)}. \tag{11.50}$$

Assuming furthermore that the calcium concentration is less than the K_d of the binding process (see Eq. 11.39) and that the pump is not saturated (that is, $[Ca^{2+}](x,t) < K_{d-pump}$), Eqs. 11.48 can be reduced (Zador and Koch, 1994; Wagner and Keizer, 1994) to

$$\frac{d(1+\beta)}{4}\frac{\partial[Ca^{2+}](x,t)}{\partial t} = \frac{d(D+\beta D_B)}{4}\frac{\partial^2[Ca^{2+}](x,t)}{\partial x^2} - P_m[Ca^{2+}](x,t) - \frac{I_{Ca}(x,t)}{2F} \tag{11.51}$$

Equation 11.51 should be very familiar to us, since it is the cable equation in disguise. To recall, the cable equation in an infinite cylinder in response to an injected current density $I_{inj}(x,t)$ is (see Eq. 2.7),

$$C_m\frac{\partial V(x,t)}{\partial t} = \frac{d}{4R_i}\frac{\partial^2 V(x,t)}{\partial x^2} - \frac{V(x,t)}{R_m} + I_{inj}(x,t). \tag{11.52}$$

If the following identifications are made, these two linear equations are identical:

$$
\begin{aligned}
R_m^{-1} &\longleftrightarrow P_m \\
R_i^{-1} &\longleftrightarrow D + \beta D_{\mathrm{B}} \\
C_m &\longleftrightarrow \frac{d(1+\beta)}{4} \\
I_{\mathrm{inj}} &\longleftrightarrow -\frac{I_{\mathrm{Ca}}}{2F}
\end{aligned}
\tag{11.53}
$$

That the pump acts like a membrane conductance R_m^{-1} is straightforward enough to understand: the more pump molecules are present, the more calcium will "leak" out of the cell. Equation 11.51 was derived under a low calcium constraint. For higher concentrations, the pump saturates (Eq. 11.47) and acts like a constant hyperpolarizing current, removing calcium ions at a constant rate.

Just as the axial resistance determines the spread of the voltage along the longitudinal axis, so does the diffusion constant determine the rate of calcium flux along the longitudinal axis (see also Fig. 11.3). The effect of a diffusible buffer is to increase the effective diffusion constant by an additive term $\beta D_{\mathrm{B}} = T_{\mathrm{B}} D_{\mathrm{B}} / K_d$. There are now two sources of calcium mobility: direct diffusion of Ca^{2+} ions and diffusion of bound calcium riding "piggyback" along with the buffer. The net effect of buffering and diffusion of the bound buffer can be expressed by a revised *effective diffusion coefficient*

$$
D_{\mathrm{eff}} = \frac{D + \beta D_{\mathrm{B}}}{1 + \beta} . \tag{11.54}
$$

(For a generalization, see Wagner and Keizer, 1994.) For the observed large binding ratio β, diffusion is dominated by the diffusion of the calcium-buffer complex.

Because calcium is measured using calcium-dependent fluorescent dyes, which themselves act as buffers for calcium ions, the perturbation of the Ca^{2+} signals by the measurement act must be taken into account (Neher, 1995).

As illustrated by Fig. 11.3, the basic diffusion equation includes an effective membrane capacitance of unity. The effect of a fast buffer is to boost this capacitance by an additive term given by the binding ratio β. Similar to a capacitance, the buffer acts to slow down changes in the calcium concentration. Note that the buffer does not affect the steady-state distribution of calcium in response to a sustained calcium current injection I_{Ca}.

11.7.2 Chemical Dynamics and Space and Time Constants of the Diffusion Equation

Further exploiting the analogy between the two equations (Zador and Koch, 1994; see also Kasai and Petersen, 1994), we know that the response of the reaction-diffusion equation to a stationary calcium current I_{Ca} in an infinite cable will be a decaying exponential, allowing us to define a space constant,

$$
\lambda_{r-d} = \sqrt{\frac{d(D + \beta D_{\mathrm{B}})}{4 P_m}} . \tag{11.55}
$$

Here r–d stands for "reaction-diffusion." We can also define a time constant associated with the linearized reaction-diffusion equation (Eq. 11.51) as

$$\tau_{r-d} = \frac{d(1+\beta)}{4P_m} \tag{11.56}$$

(see Table 11.2), with

$$D_{\text{eff}} = \frac{\lambda_{r-d}^2}{\tau_{r-d}} . \tag{11.57}$$

This similarity allows us to apply the results we derived in Chaps. 2 and 3 directly to write down equivalent expressions for the linearized reaction-diffusion equation. In particular, we can introduce the transfer "resistance" $\tilde{K}_{ij}$, defined as the ratio of the sustained change in calcium concentration at location j in response to the sustained calcium current I_{Ca} injected at location i. If locations i and j are a distance x_{ij} apart in an infinite cylinder, we have (see Eq. 3.23),

$$\tilde{K}_{ij} = \tilde{K}_{ii} e^{-x_{ij}/\lambda_{r-d}} \tag{11.58}$$

with the steady-state input resistance defined as (Eq. 3.24; see also Carnevale and Rosenthal, 1992),

$$\tilde{K}_{ii} = \frac{1}{2Fd^{3/2}\pi\sqrt{(D+\beta D_{\text{B}})P_m}} . \tag{11.59}$$

The unit of the chemical input resistance is M/A (injecting so many amperes of current increases the concentration by so many molar). From all of this we can infer a number of interesting facts.

1. As pointed out above, the buffering scheme will only affect the transient behavior, not the sustained response, acting like a capacitance. The more buffer that is present, the larger T_{B} and therefore β and thus the longer τ_{r-d}.
2. The scaling behavior of the sustained response in a cable of diameter d is identical to that of λ and $\tilde{K}_{ii}$ for the cable equation (Fig. 11.9). Because the constant in front of the pump term scales with the ratio of surface area to volume, that is, as $4/d$, and D, D_{B} and β are independent of d, λ_{r-d} scales as $\sqrt{d}$ and $\tilde{K}_{ii}$ as $d^{-3/2}$. Thus, injecting a calcium current into a small volume will give rise to a much larger change in calcium concentration than injecting the identical current into a larger volume.

$$\lambda_{r-d} \ll \lambda . \tag{11.60}$$

3. What does scale differently is the time constant. While τ_m is independent of the radius of the neuronal process, τ_{r-d} increases linearly with d (Eq. 11.56 and Fig. 11.9). Calcium

TABLE 11.2
Space and Time Constants and Input Resistance for the Linearized Reaction-Diffusion and Cable Equations

	Space constant λ	Time constant τ	Input resistance $\tilde{K}_{ii}$
Cable eq.	$\sqrt{dR_m/4R_i}$	$R_m C_m$	$d^{-3/2}\sqrt{R_m R_i}/\pi$
Reaction-diffusion eq.	$\sqrt{d(D+\beta D_{\text{B}})/4P_m}$	$d(1+\beta)/4P_m$	$d^{-3/2}/2F\pi\sqrt{(D+\beta D_{\text{B}})P_m}$

Definition of space and time constants as well as the steady-state input resistance for the cable and the linearized reaction-diffusion equation for an infinite cylinder. $\beta = T_{\text{B}}/K_d$ characterizes the buffer and P_m the ionic membrane pump. See Zador and Koch (1994).

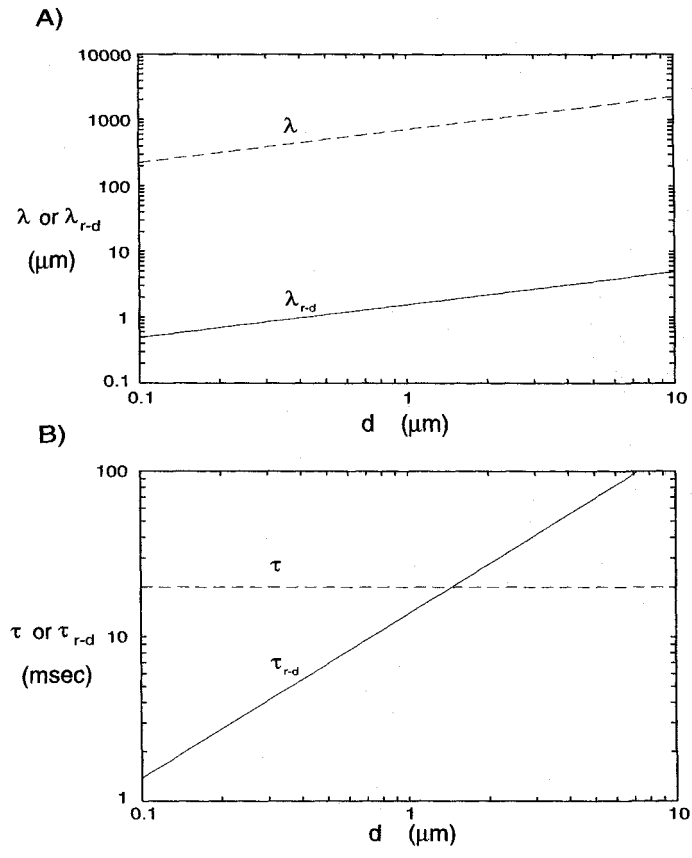

Fig. 11.9 Space and Time Constants as a Function of Cable Diameter **(A)** Space and **(B)** time constants for the linearized reaction-diffusion equation (Eq. 11.51) (solid line) and the cable equation (Eq. 2.7) (dashed line) as a function of the diameter of the infinite cable. Notice that the electrical space constant is much larger than the chemical space constant, with important functional consequences. While this is also true for the time constants for thin fibers, the time constant of the reaction-diffusion equation scales with the diameter and can therefore exceed τ_m in large structures. The parameters are chosen to mimic the binding of calcium to calmodulin. Numerical values are defined in Table 11.3. Reprinted by permission from Zador and Koch (1994).

dynamics will be slower in thicker cables than in thinner ones. (We are not, of course, accounting for radial diffusion within the cylinder, since we are only considering the one-dimensional diffusion equation.)

4. Table 11.3 lists some typical values for the space and time constants and the input resistance in an infinite cable for both Eqs. 2.7 and 11.51. What is immediately apparent is the substantial difference between the space constant of the cable equation and that of the reaction-diffusion equation,

   In other words, while voltage can act over substantial distances, the effect of the concentration of calcium (or other second messengers) is much more local. Reducing the density of calcium pumps by one, two, or even three orders of magnitude does not affect this difference dramatically. Ultimately this is due to the fact that the membrane conductances dominating the resting levels of the membrane potential (mainly K^+

TABLE 11.3
Numerical Values of λ, τ, and $\tilde{K}_{ii}$ for the Linearized Reaction-Diffusion and Cable Equations

Diameter	λ_{r-d}	τ_{r-d}	$\tilde{K}_{ii}(r-d)$	λ	τ_m	$\tilde{K}_{ii}$
0.1	0.49	1.38	84.6	224	20	14,200
1.0	1.54	13.8	26.8	707	20	450
10.0	4.88	137.5	0.085	2236	20	14.2

Space and time constants and the sustained input resistance of the reaction-diffusion and the cable equations in an infinite cable of indicated diameter (in μm) for calcium (with $D = 0.6\ \mu m^2$/msec) binding to diffusible calmodulin (with $T_B = 100\ \mu M$, $K_d = 10\ \mu M$, $\beta = 10$, and $D_B = 0.13\ \mu m^2$/msec) and in the presence of a high-affinity calcium pump ($P_m = 0.2\ \mu$m/msec). This is compared against a standard dendritic cable with $R_i = 100\ \Omega$·cm, $R_m = 20,000\ \Omega \cdot cm^2$ and $C_m = 1\ \mu F/cm^2$. Notice the dramatic difference between λ_{r-d} and λ and the different scaling behavior of τ_{r-d} and τ_m. The space constants are in units of μm and the time constants in msec. The chemical input resistance is in units of nM/fA and the electrical input resistance in MΩ.

conductances) are small relative to the interaxial resistance, while relatively more Ca^{2+} ions pass through the membrane via the pumps than flow longitudinally.

5. The dynamics of the two processes are comparable for small cylinders, but can differ greatly—due to the dependency of τ_{r-d} on the geometry—for thicker dendrites (Table 11.3 and Fig.11.9). Due to the smaller surface-to-volume ratio, the time constant of the reaction-diffusion equation can be quite slow, in the hundreds of milliseconds.

How well does the linearized reaction-diffusion equation hold up in practice? This was evaluated by observing the spread of calcium along the axon of an *Aplysia* neuron (Gabso, Neher, and Spira, 1997). Following the injection of calcium from a micropipette into the axon, calcium was tracked with the help of another fluorescent dye, fura-2, for tens of seconds as the calcium ions diffused away from the injection site for a few hundreds of micrometers.

As expressed by Eq. 2.31 and illustrated in Fig. 2.7A, the impulse response function of the cable equation in an infinite cylinder for any fixed point in time is a Gaussian. This also holds true for the linearized reaction-diffusion system we are considering,

$$[Ca^{2+}]_\delta(x,t) = \frac{A_0}{\sqrt{t}} e^{-x^2/(D_{\text{eff}}t)} e^{-t/\tau_{r-d}} \tag{11.61}$$

where the effective diffusion coefficient D_{eff} is defined in Eq. 11.57. Gabso, Neher, and Spira (1997) fit a Gaussian through the spatial profile of the calcium signal at different times (Fig. 11.10A). If the spatio-temporal dynamics of $[Ca^{2+}]$ follow Eq. 11.51, then the square of the standard deviation of the Gaussian should increase linearly in time, which it does (Fig. 11.10B). The slope of the curve gives the effective diffusion coefficient of calcium and the calcium bound to any buffers intrinsic to the axon as well as to the fura-2. Note that in this study, the calcium signal was purposely kept below 0.5 μM.

While the analogy between the cable equation and the reaction-diffusion equation breaks down for large values of calcium concentration and for more complex buffering schemes, the behavior of $[Ca^{2+}]$ will not deviate qualitatively from that described by the linear Eq. 11.51.

This is demonstrated in Fig. 11.11, which plots the normalized calcium concentration at two locations in an infinite cable for a series of calcium injections. For small currents, the system operates in the low calcium limit, and the dynamics of $[Ca^{2+}]$, obtained by solving the nonlinear coupled partial differential Eqs. 11.48, are fitted well by the linear

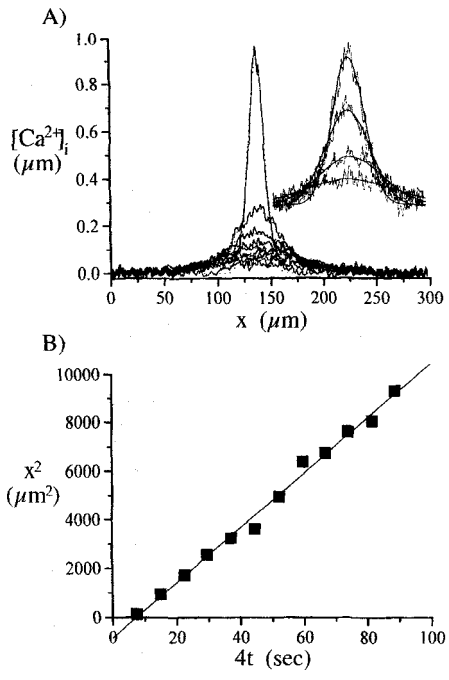

Fig. 11.10 Calcium Spread along an Axon Experimental determination of the calcium signal (recorded using the calcium-dependent fluorescent dye fura-2) following a brief intracellular injection of calcium at one point into the axon of a cultured metacerebral *Aplysia* neuron by Gabso, Neher, and Spira (1997). **(A)** Spatial profile of the $[Ca^{2+}]_i$ signal for different times. A baseline value was subtracted from each curve so that they all approach zero for large distances. Images were acquired every 1.8 sec, with the second, third, fifth, and seventh measurements displayed in the enlarged inset. A Gaussian was fitted through each curve (smooth lines in the inset). **(B)** The square of the standard deviation of the Gaussian was plotted as a function of time. If the spatio-temporal calcium dynamics follows the linearized reaction-diffusion equation (Eq. 11.51) these points should fall on a straight line whose slope is the effective diffusion coefficient D_{eff} of free and bound calcium, here equal to 0.112 μm^2/msec. Reprinted by permission from Gabso, Neher, and Spira (1997).

approximation of Eq. 11.51. As the current is made larger, the buffer saturates and becomes ineffective, since it no longer absorbs any of the inflowing calcium ions. Indeed, following Eqs. 11.37 and 11.50, at high calcium concentrations the entire buffer concentration is taken up by the bound calcium-buffer complex. Formally, this corresponds to $\beta = 0$ in Eq. 11.51, which explains the greatly spedup chemical dynamics (τ_{r-d} decreases by about one order of magnitude). However, the important point to note is that the behavior of the solutions to the full equations is bracketed by the solutions to the linear equation with $\beta = 0$ and 10, without deviating in any significant way from them (for instance, they are all monotonic, saturating functions).

The morale is that without further significant nonlinearites, our conclusions regarding the space and time constants associated with the reaction-diffusion equation do not change dramatically.

11.8 Calcium Nonlinearities

It is known that a number of different cell types exhibit all-or-none calcium events that occur over and over again (Berridge, 1990; for an excellent review of this topic see Meyer and Stryer, 1991). Such oscillations in the calcium concentration, whose duration lasts on the order of seconds or longer, can be observed in response to hormones. They have very sharp onsets and vary in frequency in a monotonic manner with the concentration of the hormone. Although these calcium spikes are on the order of three to four orders of magnitude slower than voltage spikes, they do share a number of features with their faster cousins, in particular being caused by a highly nonlinear positive feedback mechanism. Indeed, equations similar to the Hodgkin–Huxley equations have been used to replicate these experimental findings in a computer model (Meyer and Stryer, 1991; Ogden, 1996).

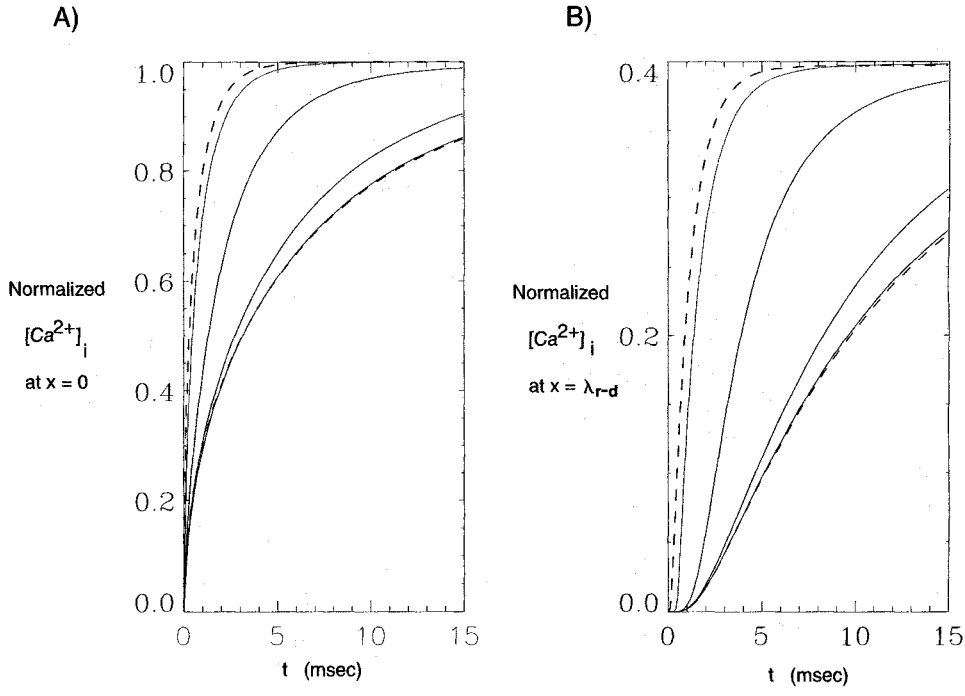

Fig. 11.11 Effect of Buffer Saturation on Calcium Diffusion Effect of saturating the buffer in an infinite cable. Plotted is the normalized calcium concentration **(A)** at the origin of the current input as well as **(B)** one space constant λ_{r-d} away. The dashed curves represent solutions to the linearized reaction-diffusion equation (Eq. 11.51) for $\beta = 10$ (lower dashed curve) and for the fully saturated buffer (corresponding to $\beta = 0$ in Eq. 11.51). The solid curves correspond to the solution of the nonlinear coupled Eqs. 11.48 for a peak calcium current of 10^{-4}, 10^{-3}, 10^{-2}, and 10^{-1} nA amplitude (from bottom to top). The behavior of the full system is bracketed by the two linear solutions; no qualitatively new behavior appears. Reprinted by permission from Zador and Koch (1994).

In some model systems, waves of increased $[Ca^{2+}]_i$ have been observed (Cornell-Bell et al., 1990; Dupont and Goldbeter, 1992; Sanderson, 1996). Applying the excitatory neurotransmitter glutamate to hippocampal *astrocytes*—non-neuronal supporting cells, which occur in great numbers throughout the brain—triggers such calcium waves, propagating at constant speeds of about 20 μm/sec throughout the cytoplasm of the astrocyte. Frequently, these waves propagate across adjacent astrocytes. The possible significance of such waves for neuronal signaling is not known.

While such nonlinear calcium events are quite intriguing, their long time scale makes it unlikely that they play a significant role in the rapid computations that we are primarily interested in.

11.9 Recapitulation

Diffusion is a fundamental fact of life for molecules in the intracellular or extracellular cytoplasm. Through its random action, it acts to move substances throughout the cell.

From a computational point of view, the most important fact about diffusion is that it places strong constraints on how rapid calcium or other second messenger molecules can affect things far away. The distance over which some concentration increase diffuses is proportional to the square root of the time that has passed. In the absence of any calcium nonlinearities and active transport processes, this square-root law fundamentally limits the ability of the calcium signal to implement the fast type of information processing operations required for many perceptual, cognitive, or motor tasks. Recognizing a friend's face, shifting visual attention from one location to a neighboring one, or raising one's hand to catch a ball can all be accomplished within a few hundred milliseconds.

The calcium that rushes into the cell via ionic channels is tightly regulated. The vast majority is bound to a host of intracellular buffers, such that only one out of 20 Ca^{2+} ions is free to interact with other molecules, severely limiting the effective diffusion coefficient of calcium.

While calcium ions diffuse along some process, their concentration rapidly decreases. This is especially true for a substance that diffuses in the three-dimensional extracellular tissue; its spatial concentration profile decreases sharply with distance from the source (as e^{-r^2}). A relevant case are certain unconventional neuroactive substances, such as *nitric oxide*, that can diffuse across the membrane cytoskeleton (Secs. 20.2 and 20.3).

Of course, these constraints do not argue against the use of the local intracellular calcium concentration for computing and for short-term memory storage (Sobel and Tank, 1994). When calcium and its protein targets are in close spatial proximity, the rate at which calcium can bind to this protein limits the speed of the computational operation being implemented (Sec. 20.1). This allows chemical switching to proceed in the submillisecond domain. Using concentration changes for implementing rapid operations does impose stringent conditions on a fast local input and a fast local read-out mechanism.

In general, movements of ions due to the inhomogeneous distribution of the various relevant ions (Ca^{2+}, Na^+, K^+ and Cl^-) must be incorporated into the cable equation, leading to the Nernst-Planck electrodiffusion equation. However, as long as the diameter of the neuronal process is above a fraction of a micrometer, this equation is well approximated by the cable equation. Only when studying very small processes, such as dendritic spines or very thin dendrites, does the longitudinal diffusion of the carriers need to be taken into account.

If the buffering reaction is substantially faster than diffusion and if the calcium concentration is small (technically, if $[Ca^{2+}]_i < K_d$ of the pump and of the buffer), the coupled system of reaction-diffusion equations can be reduced to a single linear partial differential equation, which is formally equivalent to the cable equation. This allows us to define space and time constants and input resistances in analogy to these parameters in passive dendrites. One important insight is that $\lambda_{r-d} \ll \lambda$, implying that from the point of view of spatial compartmentalization, the presence of reasonable amounts of calcium pumps and buffers in the dendritic tree will fractionate the tree into a series of small and relatively independent compartments. In each of these subunits, independent calcium-initiated chemical computations could be carried out. This is in contrast to the relatively smaller attenuation experienced by the membrane potential in a dendritic tree. It may well be possible that the architecture and morphology of the dendritic tree reflects less the need for electrical computations but more its role in isolating and amplifying chemical signals. We will study a beautiful instance of this in the following chapter on dendritic spines.

Because of the mathematical equivalence between electrical, chemical, and even biochemical networks (Busse and Hess, 1973; Eigen, 1974; Hjelmfelt and Ross, 1992; Barkai

and Leibler, 1997) that derives from their common underlying mathematical structure, appropriate sets of reaction-diffusion systems can be devised that emulate specific electrical circuits. In principle, computations can be carried out using either membrane potential as the crucial variable—controlled by the cable equation—or concentration of calcium or some other substances—controlled by reaction-diffusion equations (for examples of this, see Poggio and Koch, 1985). The principal differences are the relevant spatial and temporal scales, dictated by the different physical parameters, as well as the dynamical range of the two sets of variables. Given neuronal noise levels, the membrane potential can be considered to vary by a factor of hundred or less, while the concentration of calcium or other substances can vary by three or more orders of magnitude during physiological events.